Matter and Radiation at Extremes | RESEARCH ARTICLE | scitation.org/journal/mre

Hydrodynamical model of QED cascade expansion in an extremely strong laser pulse

Cite as: Matter Radiat. Extremes 6, 034401 (2021); doi: 10.1063/5.0035347
Submitted: 28 October 2020 • Accepted: 14 February 2021 •
Published Online: 7 April 2021

View Online Export Citation CrossMark

A. S. Samsonov,[a] I. Yu. Kostyukov, and E. N. Nerush

AFFILIATIONS

Institute of Applied Physics of the Russian Academy of Sciences, 46 Ulyanov St., Nizhny Novgorod 603950, Russia

[a]Author to whom correspondence should be addressed: asams@ipfran.ru

ABSTRACT

The development of a self-sustained quantum electrodynamical (QED) cascade in a single strong laser pulse is studied analytically and numerically. A hydrodynamical approach is used to construct an analytical model of cascade evolution, which includes the key features of the cascade observed in 3D QED particle-in-cell (QED-PIC) simulations, such as the magnetic field dominance in the cascade plasma and laser energy absorption. The equations of the model are derived in closed form and solved numerically. Direct comparison between the solutions of the model equations and 3D QED-PIC simulations shows that our model is able to describe the complex nonlinear process of cascade development qualitatively well. Various regimes of the interaction based on the intensity of the laser pulse are revealed in both the solutions of the model equations and the results of the QED-PIC simulations.

© 2021 Author(s). All article content, except where otherwise noted, is licensed under a Creative Commons Attribution (CC BY) license (http://creativecommons.org/licenses/by/4.0/). https://doi.org/10.1063/5.0035347

I. INTRODUCTION

There is strong evidence that the development of quantum electrodynamical (QED) cascades is an inherent feature of the interaction of extremely strong electromagnetic fields with matter in the majority of cases where such interactions occur.[1–11] The essence of these cascades is emission of high-energy photons by ultrarelativistic particles (nonlinear Compton scattering) and the subsequent decay of these photons into electron–positron pairs (the Breit–Wheeler process), which leads to multiplication of particles. These processes are believed to play an important role in many astrophysical phenomena, such as cosmic ray showers,[12] processes in pulsar magnetospheres,[1,2,13] and gamma-ray bursts.[14] The variety and complexity of the e^+e^- plasma structures produced in QED cascading makes it clear that there is no simple way to tackle the problem. One of the reasons behind this complexity is that the emission of photons by the electrons and positrons greatly alters the dynamics of the latter—an effect known as radiation reaction. Obtaining an accurate description of radiation reaction is a longstanding problem in both classical and quantum electrodynamics.[15–18]

With the upcoming multi-petawatt laser facilities such as ELI[19] and Apollon,[20] these processes are expected to be observed in light–matter interaction experiments in the laboratory. An extensive search for the optimal configuration for such experiments is currently being conducted.[21–27] As already mentioned, the significantly nonlinear nature of the QED cascade complicates its analytical study, and while particle-in-cell (PIC) simulations serve as a starting point for most theoretical research and can give valuable insight into the nature of the processes involved, even the derivation of phenomenological descriptions or scaling laws can be extremely time-consuming because of the need in most cases for a scan over the multidimensional map of parameters. These dependences, however, are crucial for the design of experiments to be carried out on the next generation of laser facilities. Various schemes have been proposed to lower the threshold of QED cascading.[8,24,25,28–34] One such scheme involves the use of multiple laser pulses with small numbers of seed particles, while another takes advantage of laser–beam interaction. The key reason why these configurations are optimal is that the governing parameter of the QED processes, χ, which is the ratio of the transverse component of the effective electric field experienced by the relativistic particle in the rest frame to the critical Sauter–Schwinger field,[35] is maximized in these scenarios. There is a crucial difference, though, between these two approaches: in the first case, the cascade gains its energy from the electromagnetic field and is called an A-type cascade, while in the second case, the cascade energy is mostly limited by the initial energy of the seed in what is called an S-type cascade.[36]

Exploration of these schemes lies beyond the scope of this paper. Instead, we further investigate a specific configuration of QED cascade development that occurs in a *single* extremely intense laser pulse and that can be initiated during interaction with a motionless seed. This type of cascade has been recently explored by three-dimensional

(3D) QED-PIC simulations in Ref. 37. The peculiar mechanism of this cascade development makes it difficult to assign it as either an A-type or S-type cascade. For the sake of convenience, we will briefly describe the core mechanism of the discussed cascade (see Fig. 1 for a schematic of the process). The main feature that allows the cascade to sustain itself is the fact that the collective motion of the electrons and positrons alters the laser field so that its magnetic component becomes larger than its electric component while they remain nearly mutually perpendicular. In such fields, particles drift along the direction of laser propagation with the drift velocity and rotate in the plane perpendicular to the direction of the magnetic field, and so their trajectories are helical (see the supplementary material). The particles radiate gamma quanta along the direction of the instantaneous tangent to the trajectory. Occasionally, that direction may be opposite to the direction of laser propagation. Such gamma quanta eventually leave the electron–positron plasma and reach the vacuum, where a strong laser field is present and where they are highly likely to photoproduce new electron–positron pairs. The newly created pairs are then accelerated by the laser pulse and pushed toward the plasma region, and the process repeats. As a result, the QED cascade continuously expands toward the laser pulse, building a pair plasma "cushion." This process is similar to the propagation of the ionization front in the microwave gas discharge.[38] It is important to stress the major difference between the *vacuum* and *plasma* regions: in the former, the electromagnetic energy is transferred to the cascade particles, while in the latter, the particles are not accelerated but release the gained energy in the form of gamma radiation. Some portion of this radiation returns to the vacuum region and provides the positive feedback that is essential for the cascade to be able to sustain itself.

Models describing the electrodynamics of the cushion plasma[37,39] and QED cascade evolution[37] have been proposed. However these models are not self-consistent. The model proposed in Ref. 39 does not take into account particle multiplication due to cascading, while the model in Ref. 37 neglects laser field depletion due to absorption in the cascade plasma. In this paper, we construct a self-consistent model that describes the spatiotemporal evolution of both the laser field and the cascade plasma. The goal of the paper is twofold. First, we develop a reduced model that requires much less in the way of computational resources than are needed for 3D QED-PIC simulations. Second, the model development and its verification allow us to understand and evaluate the roles of the different physical processes underlying QED cascading in a single laser pulse.

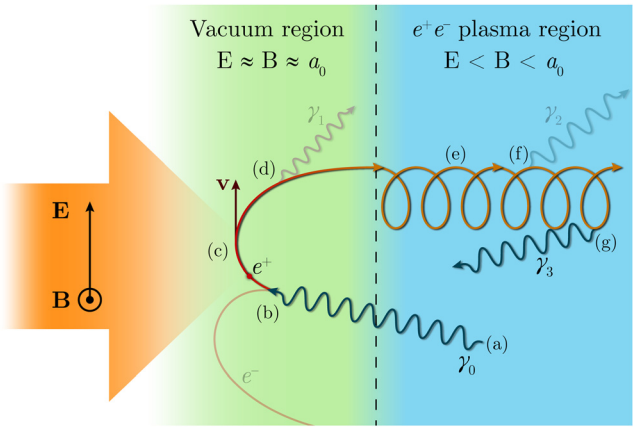

FIG. 1. Core mechanism of cascade self-sustenance. (a), (f), and (g) Emission of a gamma quantum in the plasma region or the *involved* gamma quantum. (b) Decay of the *involved* gamma quantum in the vacuum region. (c) Positron and electron acceleration in the plane wave. (d) Emission of the gamma quantum in the vacuum region or the *decoupled* gamma quantum. (e) Helical motion of the positron in the plasma region.

The remainder of the paper is organized as follows. In Sec. II, we formulate the problem and start from the kinetic equations, including QED processes. Next, we propose a set of general simplifications that allow a great reduction in the complexity of the equations. On the basis of these simplifications, self-consistent hydrodynamical equations are derived. In Sec. III, the method of numerical solution of the derived equations is discussed, and the results of this solution are compared with those of QED-PIC simulations. The obtained results are summarized and discussed in Sec. IV. In Appendix A, we examine the problem of single-electron acceleration in a plane wave, and in Appendix B, we derive the electrodynamical properties of a dense electron–positron plasma. The results for both these problems are used in the derivation of the model equations.

II. DERIVATION OF MODEL OF QED CASCADE DEVELOPMENT

Similarly to Refs. 28 and 40, we start our analysis from the kinetic equations for electrons, positrons, and gamma quanta, assuming that the QED cascade is in its self-sustaining stage and so the seed particles (e.g., the electrons and the ions of the target) do not contribute to it. The kinetic equations and Maxwell's equations can be written as follows:

$$\frac{\partial f_{e^\pm}}{\partial t} + \mathbf{v}_{e^\pm}\cdot\nabla f_{e^\pm} \pm [\mathbf{E} + (\mathbf{v}_{e^\pm}\times\mathbf{B})]\cdot\frac{\partial f_{e^\pm}}{\partial \mathbf{p}} = \int f_\gamma(\mathbf{p}')w_{\mathrm{pair}}(\mathbf{p}',\mathbf{p})\,d\mathbf{p}' + \int f_{e^\pm}(\mathbf{p}')w_{\mathrm{rad}}(\mathbf{p}',\mathbf{p})\,d\mathbf{p}' - \int f_{e^\pm}(\mathbf{p})w_{\mathrm{rad}}(\mathbf{p},\mathbf{p}')\,d\mathbf{p}', \tag{1}$$

$$\frac{\partial f_\gamma}{\partial t} + \mathbf{v}_\gamma\cdot\nabla f_\gamma = \int f_{e^\pm}(\mathbf{p}')w_{\mathrm{rad}}(\mathbf{p}',\mathbf{p}'-\mathbf{p})\,d\mathbf{p}' - \int f_\gamma(\mathbf{p})w_{\mathrm{pair}}(\mathbf{p},\mathbf{p}')\,d\mathbf{p}', \tag{2}$$

$$\nabla\times\mathbf{E} = -\frac{\partial\mathbf{B}}{\partial t}, \tag{3}$$

$$\nabla\times\mathbf{B} = \frac{\partial\mathbf{E}}{\partial t} + \int f_{e^+}\mathbf{v}_{e^+}\,d\mathbf{p} - \int f_{e^-}\mathbf{v}_{e^-}\,d\mathbf{p}, \tag{4}$$

where $f_{e^\pm,\gamma}(t,\mathbf{r},\mathbf{p})$ are the distribution functions of the electrons, positrons, and gamma quanta, respectively, $\mathbf{v}$ is the particle velocity (which is equal to $\mathbf{p}/\sqrt{1+p^2}$ for electrons and positrons and to $\mathbf{p}/p$ for gamma quanta), $w_{\mathrm{rad}}(\mathbf{p}',\mathbf{p})\,d\mathbf{p}'$ is the probability per unit time for an electron or positron with momentum $\mathbf{p}'$ to emit a gamma quantum

©Author(s) 2021

with momentum $\mathbf{p}' - \mathbf{p}$, and $w_{\text{pair}}(\mathbf{p}', \mathbf{p})\, d\mathbf{p}'$ is the probability per unit time for a gamma quantum with momentum $\mathbf{p}'$ to photoproduce an electron with momentum $\mathbf{p}$ and a positron with momentum $\mathbf{p}' - \mathbf{p}$. We use the common relativistic normalization in which the electric and magnetic fields are normalized to the value of $m_e c\omega_L/e$ (where m_e and $e > 0$ are the mass and charge of the electron, c is the speed of light, and ω_L is the characteristic frequency of the external field), the particle number densities are normalized to the critical density $n_{\text{cr}} = m_e\omega_L^2/4\pi e^2$, the energies and momenta are normalized to $m_e c^2$ and $m_e c$, respectively, and the coordinates and time are normalized to c/ω_L and $1/\omega_L$, respectively (and thus the velocities are normalized to c).

A. Model assumptions

We adopt several assumptions to simplify the model. First of all, as we are investigating interaction with a plane electromagnetic wave, the problem can be considered to be spatially one-dimensional. If we also restrict ourselves to circularly polarized laser pulses, then the symmetry with respect to rotation about the axis of pulse propagation (the x axis hereinafter) can also be utilized. These simplifications lead to the distribution functions becoming dependent on three variables (excluding time) rather than six: $f(t; \mathbf{r}, \mathbf{p}) = f(t; x, p, \theta)/2\pi$, where p is the momentum of the particle and θ is the angle between the momentum and the x axis.

Second, we will assume all distribution functions to be locally monoenergetic, i.e., $f \propto \delta(p - \overline{p}(x))/p^2$, where $\overline{p}(x)$ is the mean value of the momentum of the particles located in a small vicinity of x. We denote the mean energy of gamma quanta by ε_γ and the mean energy of pairs by ε_p, assuming that particles are ultrarelativistic and thus $\varepsilon_p^2 = 1 + p_p^2 \approx p_p^2$. While the monoenergetic approximation is quite strong, we suppose that the mechanism of cascade development explained in Sec. I does not rely on any particular feature of the particles' energy spectra. Therefore, we argue that taking account of the evolution of energy spectra in our model will lead to only quantitative changes rather than qualitative ones, while greatly complicating the equations. It will be discussed later how this assumption is valid for the pairs that enter the plasma region with approximately equal energies. For the gamma quanta, we actually use a two-stream approximation, i.e., we separate gamma quanta into those that are emitted in the vacuum region and propagate mostly along the direction of laser pulse propagation and thus do not contribute to the cascade (we designate them as *decoupled* gamma quanta) and those that are emitted in the plasma region in many different directions and provide the positive feedback needed for cascade development (we designate them as either *involved* gamma quanta or simply gamma quanta). As Fig. 2 shows, the energy spectrum of the gamma quanta is broad, while if we exclude the *decoupled* gamma quanta, then the width of the spectrum decreases significantly, which justifies our assumption. As the *decoupled* gamma quanta affect the cascade development only by taking away some portion of the total energy, their spatial distribution is irrelevant for the cascade, but it will be calculated to allow more explicit comparison with the results of the QED-PIC simulations.

To omit integration over energies and the azimuth angle φ, we redefine f as follows:

$$f(x, \varepsilon, \theta, \varphi) \to \int_0^\infty \int_0^{2\pi} f(x, \varepsilon, \theta, \varphi) 2\pi\varepsilon^2\, d\varphi\, d\varepsilon = n(x)\Phi(\theta). \quad (5)$$

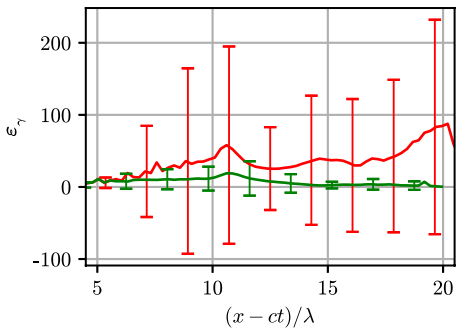

FIG. 2. Mean energy ϵ_γ of gamma quanta located in the vicinity of the x coordinate calculated from all the particles (red line) and from the particles with velocity along the x axis less than 0.5, which supposedly include only the *involved* gamma quanta (green line). The error bars depict the standard deviation. The data are taken from the results of the PIC simulation for the time instant $ct/\lambda = 18$. The simulation parameters are discussed in Sec. III. The initial conditions are the same as in Fig. 6.

where $n(x)$ is the particle density distribution and $\Phi(\theta)$ is the particle angular momentum distribution, which are such that

$$\int_{-\infty}^{+\infty} n(x)\, dx = N, \quad (6)$$

$$\int_0^\pi \Phi(\theta) \sin\theta\, d\theta = 1, \quad (7)$$

where N is the total number of particles. The assumption of a monoenergetic distribution suggests that we can use a hydrodynamical approach by calculating the moments of the distribution functions from Eqs. (1) and (2). The following quantities can be introduced:

$$W_{\text{pair}}(\chi_\gamma, \varepsilon_\gamma) = \int w_{\text{pair}}(\mathbf{p}, \mathbf{p}')\, d\mathbf{p}', \quad (8)$$

$$W_{\text{rad}}(\chi_p, \varepsilon_p) = \int w_{\text{rad}}(\mathbf{p}, \mathbf{p}')\, d\mathbf{p}', \quad (9)$$

$$I_{\text{rad}}(\chi_p) = \int w_{\text{rad}}(\mathbf{p}, \mathbf{p}')(\varepsilon_p - \varepsilon_p')\, d\mathbf{p}', \quad (10)$$

where W_{pair} and W_{rad} are the total probabilities of pair photoproduction and of gamma-quanta emission, respectively, and I_{rad} is the intensity of gamma radiation.[18] Note that these quantities depend on the Lorentz-invariant QED parameter χ, which is given by

$$\chi = \frac{\varepsilon}{\mathcal{E}_S}\sqrt{(\mathbf{E} + \mathbf{v} \times \mathbf{B})^2 - (\mathbf{v} \cdot \mathbf{E})^2}, \quad (11)$$

where ε is the particle energy, $\mathcal{E}_S = eE_S/m_e c\omega_L = m_e c^2/\hbar\omega_L$, and $E_S = m_e{}^2 c^3/\hbar e$ is the critical Sauter–Schwinger field.[35]

Generally the hydrodynamical equations have the form of a continuity equation, i.e.,

$$\frac{\partial D_\alpha}{\partial t} + \frac{\partial F_\alpha}{\partial x} = \sum_\beta S[\alpha, \beta], \quad (12)$$

where D_α and F_α are the density and flux of some quantity α, and $S[\alpha, \beta]$ is the source responsible for changes in α in the process β. Note that

© Author(s) 2021

despite the fact that we have specified the energy distribution of the particles, to calculate the sources $S[\alpha, \beta]$ we also need to know the angular distribution of the particles, which will be discussed below. We suppose that the following set of equations can quantitatively describe the cascade development:

$$\frac{\partial}{\partial t}n_p + \frac{\partial}{\partial x}(v_x n_p) = S[n, \mathrm{pp}], \tag{13}$$

$$\frac{\partial}{\partial t}(\varepsilon_p n_p) + \frac{\partial}{\partial x}(v_x \varepsilon_p n_p) = S[\varepsilon, \mathrm{pp}] + S[\varepsilon, \mathrm{acc}]\psi_{\mathrm{vac}} - S[\varepsilon, \mathrm{rad}_i]\psi_{\mathrm{pl}} - S[\varepsilon, \mathrm{rad}_d]\psi_{\mathrm{vac}}, \tag{14}$$

$$\frac{\partial}{\partial t}n_\gamma + \frac{\partial}{\partial x}\left(\overline{v_{\gamma\|}}n_\gamma\right) = -S[n, \mathrm{pp}] + 2S[n, \mathrm{rad}_i]\psi_{\mathrm{pl}}, \tag{15}$$

$$\frac{\partial}{\partial t}\left(\overline{v_{\gamma\|}}n_\gamma\right) + \frac{\partial}{\partial x}\left(\overline{v^2_{\gamma\|}}n_\gamma\right) = -S[v, \mathrm{pp}] + 2S[v, \mathrm{rad}_i]\psi_{\mathrm{pl}}, \tag{16}$$

$$\frac{\partial}{\partial t}\left(\varepsilon_\gamma n_\gamma\right) + \frac{\partial}{\partial x}\left(\overline{v_{\gamma\|}}\varepsilon_\gamma n_\gamma\right) = -S[\varepsilon, \mathrm{pp}] + 2S[\varepsilon, \mathrm{rad}_i]\psi_{\mathrm{pl}}, \tag{17}$$

$$\frac{\partial}{\partial t}\left(\frac{E^2 + B^2}{2}\right) + \frac{\partial}{\partial x}(\mathbf{E}\times\mathbf{B})_x = -2S[\varepsilon, \mathrm{acc}]\psi_{\mathrm{vac}} \equiv -\mathbf{j}\cdot\mathbf{E}, \tag{18}$$

$$\frac{\partial \Sigma_\gamma}{\partial t} = 2\int_0^\infty S[\varepsilon, \mathrm{rad}_d]\psi_{\mathrm{vac}}dx, \tag{19}$$

where $n_p = n_{e^+} = n_{e^-}$ is half the density of the electron–positron plasma under the assumption that the cascade plasma is quasineutral, v_x is the mean longitudinal velocity of the pairs, which is calculated in Sec. II E, and $\overline{v_{\gamma\|}}$ and $\overline{v^2_{\gamma\|}}$ are the mean longitudinal velocity and mean square longitudinal velocity of the gamma quanta, which are calculated from their angular distribution as follows:

$$\overline{v_{\gamma\|}} = \int_0^\pi \Phi(\theta)\cos\theta \sin\theta\, d\theta, \tag{20}$$

$$\overline{v^2_{\gamma\|}} = \int_0^\pi \Phi(\theta)\cos^2\theta \sin\theta\, d\theta. \tag{21}$$

Equation (18) is Poynting's theorem, which is essentially the continuity equation for the electromagnetic energy density. The sources $S[n, \beta]$, $S[v, \beta]$, and $S[\varepsilon, \beta]$ correspond to the changes in particle density, longitudinal velocity, and energy, respectively, and the sources $S[\alpha, \mathrm{pp}]$, $S[\alpha, \mathrm{acc}]$, $S[\alpha, \mathrm{rad}_i]$, and $S[\alpha, \mathrm{rad}_d]$ correspond to the processes of pair photoproduction, pair acceleration in the electromagnetic field, *involved* gamma-quanta emission by pairs in the plasma region, and *decoupled* gamma-quanta emission by pairs in the vacuum region, respectively [labeled (b), (c), (d), and (f), respectively in Fig. 1]. Σ_γ is the total energy of the *decoupled* gamma quanta. The factor ψ_{vac} (respectively ψ_{pl}) is equal to 1 in the vacuum (respectively plasma) region and to 0 in the plasma (respectively vacuum) region. These factors will be specified below. Note that $\psi_{\mathrm{vac}} + \psi_{\mathrm{pl}} = 1$. For the sake of convenience, these factors will be omitted where it is clear what region is being discussed.

B. Electromagnetic field configuration

According to the results of 3D QED-PIC simulations, the electric and the magnetic fields inside the plasma region remain almost mutually perpendicular and the magnitude of the magnetic field is everywhere larger than that of the electric field ($B > E$). The spatial distribution of the electromagnetic field has a characteristic scale of λ in both regions. In such a field configuration, a charged particle drifts perpendicularly to both the electric and magnetic fields with velocity $\mathbf{v_d} = \mathbf{E}\times\mathbf{B}/B^2$. Under the assumption that the laser pulse propagates along the x axis and thus the fields lie in the yz plane, this velocity is directed along the x axis. Assuming that the fields are mutually perpendicular, we get

$$v_x \approx E/B. \tag{22}$$

In the vacuum region, the fields are close to those of a plane wave, i.e., the electric and magnetic fields are approximately equal in magnitude ($E \approx B$) and are nearly mutually perpendicular ($\mathbf{E}\cdot\mathbf{B} \approx 0$). If the initial energy of the particle ε is smaller than the field amplitude E, then on timescales much shorter than the laser period, the longitudinal velocity of the particle tends to the speed of light, i.e., $v_x \approx 1 = E/B$ (see Appendix A). So, we assume that Eq. (22) is valid in both the vacuum and plasma regions.

We do not account for reflected waves in our model, for several reasons. First of all, no significant reflection during the cascade development during the stage of its self-sustenance is observed in 3D QED-PIC simulations. Second, the reflection that occurs during the initial stage of laser interaction with a thin solid target quickly decreases according to the theory of relativity, since particles are being accelerated in the direction of laser pulse propagation, and thus it becomes insignificant during the later stages of cascade development. Our model is not suitable for describing an electron–ion plasma, though, so we investigate the interaction of the laser pulse with a seed in the form of a counter-propagating gamma bunch where no reflection occurs even during the initial stage of the interaction (see Sec. III). Moreover, reflection would insignificantly alter the process of pair photoproduction owing to the fact that gamma quanta with the highest probability of decay counter-propagate with respect to the incident laser pulse, i.e., co-propagate with respect to the reflected radiation. However, the fields of the co-propagating wave do not alter the governing QED parameter χ of the gamma quanta. Lastly, in the vacuum region, where the laser field is strongest, it is mostly ultrarelativistic electrons and positrons that are being born, because higher-energy photons have a higher probability of pair photoproduction. Scattering of a relativistically strong laser field ($a_0 \gg 1$) on ultrarelativistic electrons and positrons ($\gamma \gg 1$) occurs in both a nonlinear and quantum regime. Because of this, and the fact that the particles' initial coordinates are uncorrelated, their resulting radiation is incoherent and its frequency is highly upshifted. Such radiation is best described in terms of individual photons. The portion of these photons counter-propagating with respect to the laser pulse can indeed be considered as reflection. While such photons can enhance the total yield of electron–positron pairs and gamma quanta through QED processes of higher order, they are significantly less probable than nonlinear Compton scattering and the Breit–Wheeler process and thus are not taken into account in either QED-PIC simulations or in our model. Note, though, that the energy loss due to incoherent

© Author(s) 2021

gamma radiation in both the vacuum and plasma regions is accounted for in our model.

C. Involved gamma-quanta distribution function

As discussed in Sec. I, the *involved* gamma quanta are emitted by pairs during their motion along helical trajectories in the plasma region (see the pair tracks in the supplementary material). Because of this, the angular distribution of the gamma quanta is quite wide. We will assume that it is smooth and can be described by a single parameter. This parameter is the velocity v of the instantaneous reference frame K' in which the angular distribution of the particles located in the vicinity of the x coordinate is uniform, i.e.,

$$\Phi'(\theta') \equiv \frac{dN'}{d\cos\theta'} = \frac{1}{2}, \tag{23}$$

where $dN' = dN$ is the number of particles with longitudinal velocities in the range $[\cos\theta', \cos\theta' + d\cos\theta']$ and

$$\cos\theta' = \frac{\cos\theta - v}{1 - v\cos\theta}. \tag{24}$$

In the laboratory reference frame, this transforms into[41]

$$\Phi(\theta, v) = \frac{dN}{d\cos\theta} = \frac{dN'}{d\cos\theta'}\frac{d\cos\theta'}{d\cos\theta} = \frac{1 - v^2}{2(1 - v\cos\theta)^2}. \tag{25}$$

So, the total distribution function of the *involved* gamma quanta has the form

$$f_\gamma(t; x, \theta) = \Phi\big(\theta, v_{\gamma\|}(x,t)\big) n_\gamma(x,t). \tag{26}$$

The mean velocity $\overline{v_{\gamma\|}}$ and the mean square velocity $\overline{v_{\gamma\|}^2}$ are

$$\overline{v_{\gamma\|}} = \int_0^\pi \Phi(\theta, v)\cos\theta\sin\theta\, d\theta = \frac{1}{v_{\gamma\|}} - \frac{1 - v_{\gamma\|}^2}{v_{\gamma\|}^2}\operatorname{artanh}(v_{\gamma\|}), \tag{27}$$

$$\overline{v_{\gamma\|}^2} = \int_0^\pi \Phi(\theta, v)\cos^2\theta\sin\theta\, d\theta = \frac{2\overline{v_{\gamma\|}}}{v_{\gamma\|}} - 1. \tag{28}$$

Note that owing to Lorentz transformation, the mean longitudinal velocity of the gamma quanta, $\overline{v_{\gamma\|}}$, differs from the velocity $v_{\gamma\|}$ of the reference frame in which their distribution is uniform. The results of the QED-PIC simulations show that Eq. (25) is a good approximation for the angular distribution of the *involved* gamma quanta [see Figs. 3(a) and 3(b)].

The χ parameter of the gamma quanta propagating in crossed electric and magnetic fields, which is the case for both the plasma and vacuum regions, can be calculated as follows:

$$\chi_\gamma = \frac{\varepsilon_\gamma |B - E\cos\theta|}{\mathcal{E}_S} = \frac{\varepsilon_\gamma E}{\mathcal{E}_S}\frac{1 - v_x\cos\theta}{v_x}, \tag{29}$$

where we have used Eq. (22).

Having specified the distribution function of the gamma quanta completely, it is possible to calculate the sources $S[\alpha, \mathrm{pp}]$ that correspond to the process of pair photoproduction:

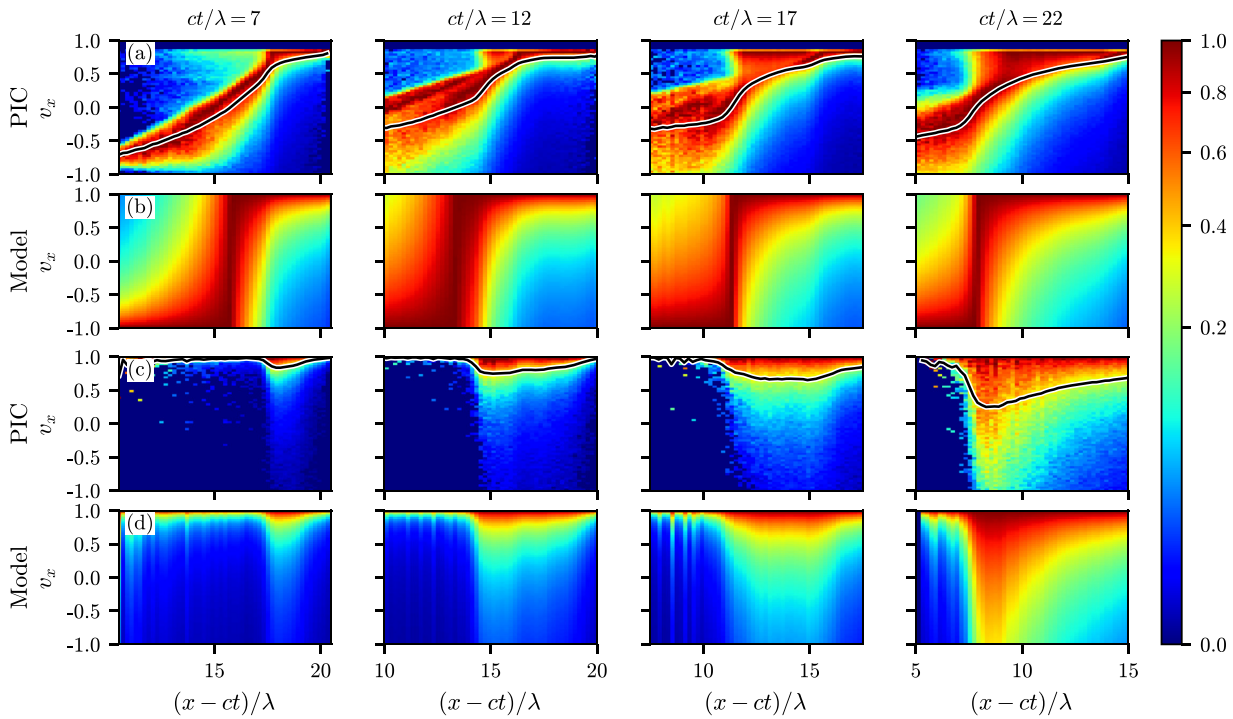

FIG. 3. Validation of the approximation used for describing angular distribution of the particles. (a) and (c) Angular distributions of gamma quanta (a) and pairs (c) located in the vicinity of the coordinate x (color map) and the mean longitudinal velocity calculated from the distribution (black line) computed from the results of the QED-PIC simulation. (b) and (d) Angular distributions of gamma quanta (b) and pairs (d) calculated from the mean velocity using the expression (25).

©Author(s) 2021

$$S[n,\mathrm{pp}] = n_\gamma \int_0^\pi \Phi(\theta, v_{\gamma\parallel}) W_{\mathrm{pair}}(\chi_\gamma, \varepsilon_\gamma) \sin\theta\, d\theta \equiv \overline{W_{\mathrm{pair}}} n_\gamma, \quad (30)$$

$$S[\varepsilon,\mathrm{pp}] = \varepsilon_\gamma n_\gamma \int_0^\pi \Phi(\theta, v_{\gamma\parallel}) W_{\mathrm{pair}}(\chi_\gamma, \varepsilon_\gamma) \sin\theta\, d\theta \equiv \overline{W_{\mathrm{pair}}} \varepsilon_\gamma n_\gamma, \quad (31)$$

$$S[v,\mathrm{pp}] = n_\gamma \int_0^\pi \Phi(\theta, v_{\gamma\parallel}) W_{\mathrm{pair}}(\chi_\gamma, \varepsilon_\gamma) \cos\theta \sin\theta\, d\theta \equiv \overline{V_{\mathrm{pair}}} n_\gamma. \quad (32)$$

D. Pair dynamics in the vacuum region

Let us examine the electrons and positrons located in the vacuum region, where the number of particles is small and so collective plasma effects can be neglected. Thus, the electromagnetic field in that region coincides with the field of the incident radiation. In our case, those electrons and positrons that are born in the vacuum region move in the field of a plane electromagnetic wave. The dynamics of a single particle in a plane wave is discussed in Appendix A. Computing the sources $S[\alpha, \beta]$ on the right-hand sides of Eqs. (13)–(18) requires knowledge of the particle distribution function. Although approximate particle trajectories can be found analytically, deriving an explicit expression for the distribution function is not feasible in practice owing to the fact that particles are being born at different time instants with varying initial conditions. However, a few observations will allow us to estimate $S[\alpha, \beta]$ using a different approach. The first observation is that a strong electromagnetic plane wave pushes particles in the direction of its propagation, i.e., the x axis. Therefore, after some time interval, independently on its initial direction, the particle momenta are oriented almost parallel to the x axis, and so $v_x \approx 1$ [see Fig. 1(c) and Eq. (A37)]. We neglect the duration of this momentum orientation, which allows us to approximate the fluxes of particle density and energy density by simply multiplying these densities by the velocity $v_x \approx 1$.

The purpose of the continuity equations in the vacuum region is essentially to provide the values of the particle densities and energies and the magnitude of the electric field at the plasma–vacuum interface (which we will occasionally call the cascade front). Thus, we are interested in the total contribution to these values from each particle during its motion from the moment of its birth in the vacuum region up to the moment at which it reaches the plasma boundary. We do this by defining the sources $S[\varepsilon, \beta]$ in the following way:

$$S[\varepsilon,\beta] = \int_0^\pi f_\gamma(x,\theta) W_{\mathrm{pair}}(\chi_\gamma, \varepsilon_\gamma) \Delta\varepsilon_\beta \sin\theta\, d\theta, \quad (33)$$

where $\Delta\varepsilon_\beta$ is the total change in energy due to the process β of a single particle born at the point in space with coordinate x at time instant t while the particle stays in the vacuum region.

The energy gained by a single particle in the plane wave can be evaluated as

$$\Delta\varepsilon_{\mathrm{acc}} = \mu 2^{1/3} E^{2/3} \varepsilon_0^{1/3} (1-\cos\theta)^{1/3}, \quad (34)$$

where ε_0 is the initial particle energy and μ is a parameter determining the time the particle spends in the vacuum region (see Appendix A). This parameter depends on the time of particle birth and the time at which the particle crosses the plasma boundary. Finding the latter requires either constructing an independent model of cascade front propagation or finding some heuristics, both of which lie outside the scope of this paper. Instead, we suppose that μ is constant during the whole cascade development and that its value can be estimated by comparing the results of the model with the results of QED-PIC simulations, and thus μ is the first fitting parameter of our model. Noting that when pairs are born from gamma quanta their average initial energy is approximately equal to half the energy of the parent gamma quanta ε_γ, we derive the following expression for $S[\varepsilon, \mathrm{acc}]$:

$$\begin{aligned} S[\varepsilon,\mathrm{acc}] &= E^{2/3} \varepsilon_\gamma^{1/3} \mu n_\gamma \int_0^\pi \Phi(\theta, v_{\gamma\parallel}) W_{\mathrm{pair}}(\chi_\gamma, \varepsilon_\gamma) \\ &\quad \times (1-\cos\theta)^{1/3} \sin\theta\, d\theta \\ &\equiv E^{2/3} \varepsilon_\gamma^{1/3} \mu \overline{G_{\mathrm{rad}}} n_\gamma. \end{aligned} \quad (35)$$

Validation of this approximate expression is shown in Fig. 4(a). Note that absorption is large in the vacuum region, where the pair density is small, and is almost negligible in the dense plasma region, as discussed in Sec. I. Also note that the approximate value is shifted along the x axis, which corresponds to the fact that we compute $\mathbf{j}\cdot\mathbf{E}$ as if the particle absorbed all the energy at the moment of its birth, whereas actually $\mathbf{j}\cdot\mathbf{E}$ is gained during all the time the particle spends in the vacuum region [see Eq. (A30)].

The total energy loss due to photon emission of a single particle can be calculated as follows (see Appendix A):

$$\Delta\varepsilon_{\mathrm{rad}} = \int_0^{\sqrt{4\mu^3/9}} I_{\mathrm{rad}}(\chi)\, dt, \quad (36)$$

with

$$\frac{d\chi}{dt} = -\frac{\chi_0}{\varepsilon_0 + \left[\frac{9}{2} E^2 \varepsilon_0 t^2 (1-\cos\theta)\right]^{1/3}} I_{\mathrm{rad}}(\chi), \quad (37)$$

$$\chi_0 = \frac{1}{2}\chi_\gamma, \qquad \varepsilon_0 = \frac{1}{2}\varepsilon_\gamma. \quad (38)$$

Therefore, the source term $S[\varepsilon_p, \mathrm{rad}]$ takes the form

$$S[\varepsilon_p,\mathrm{rad}] = n_\gamma \int_0^\pi \Phi(\theta, v_{\gamma\parallel}) W_{\mathrm{pair}}(\chi_\gamma, \varepsilon_\gamma) \Delta\varepsilon_{\mathrm{rad}} \sin\theta\, d\theta \equiv \overline{I_{\mathrm{vac}}} n_\gamma. \quad (39)$$

E. Pair dynamics in the plasma region

In the plasma region, at each point in space, there exists an instantaneous reference frame K' moving with velocity $v_x(x,t) \approx E/B$ in which only a magnetic field is present. It is convenient to obtain some results in that reference frame. In the frame K', electrons and positrons move along the magnetic field with velocity v_B' and rotate in the plane perpendicular to it with velocity $v_\perp'$ (see Fig. 5). We will assume that the particles remain ultrarelativistic in that reference frame, and so $v_\perp'^2 + v_B'^2 \approx 1$. Motion along the magnetic field results in a nonzero average current, which has to be taken into account in Maxwell's equations, while rotation in the magnetic field gives zero average current but is responsible for producing gamma quanta. In particular, the Lorentz-invariant QED parameter χ for pairs can be written as

$$\chi_p = \frac{v_\perp' \varepsilon_p' B'}{E_S}. \quad (40)$$

We express the primed values through the values in the laboratory reference frame as $B' = B\sqrt{1-(E/B)^2}$ and $\varepsilon_p' = \varepsilon_p \sqrt{1-(E/B)^2}$, where we have used the facts that the average particle momentum

© Author(s) 2021

along the x axis is equal to γv_x and that $v_x = E/B$. The final form of the expression for χ is

$$\chi_e = \frac{v_\perp' \varepsilon_p E}{E_S} \frac{1 - v_x^2}{v_x}. \tag{41}$$

Owing to the rotation of the particles around the direction of the magnetic field, we can assume that their angular distribution in the reference frame K' is close to uniform. Applying a Lorentz transformation, we derive the following distribution function of pairs in the laboratory reference frame:

$$f_p(t, x, \theta) = \Phi(\theta, v_x(x, t)) n_p(x, t), \tag{42}$$

where Φ is defined the same way as in Eq. (25):

$$\Phi(\theta, v) = \frac{1 - v^2}{2(1 - v\cos\theta)^2}. \tag{43}$$

Similarly to the gamma quanta, the results of the QED-PIC simulations demonstrate that Eq. (42) is a good approximation for the angular distribution of the pairs [see Figs. 3(c) and 3(d)]. We will show below that the velocity v_x can be calculated from the local values of the electric field and plasma density. That is why we do not include a continuity equation for the density of the longitudinal velocity of the pairs similar to Eq. (16). Also, in the case of the pairs, we choose to neglect the difference between the velocity v of the reference frame in which the particle angular distribution is uniform and the actual mean velocity $\bar{v}$ calculated from that distribution, the maximum difference between which is less than 0.2, according to Eq. (27).

Because χ_p does not depend on θ, we calculate the sources $S[\alpha, \mathrm{rad}_i]$ as follows:

$$S[n, \mathrm{rad}_i] = n_p \int_0^\pi \Phi(\theta, v_x) W_{\mathrm{rad}}(\chi_p, \varepsilon_p) \sin\theta \, d\theta = W_{\mathrm{rad}}(\chi_p, \varepsilon_p) n_p \equiv \overline{W_{\mathrm{pl}}} n_p, \tag{44}$$

$$S[\varepsilon, \mathrm{rad}_i] = n_p \int_0^\pi \Phi(\theta, v_x) I_{\mathrm{rad}}(\chi_p) \sin\theta \, d\theta = I_{\mathrm{rad}}(\chi_p) n_p \equiv \overline{I_{\mathrm{pl}}} n_p, \tag{45}$$

$$S[n, \mathrm{rad}_i] = n_p \int_0^\pi \Phi(\theta, v_x) \cos\theta W_{\mathrm{rad}}(\chi_p, \varepsilon_p) \sin\theta \, d\theta = W_{\mathrm{rad}}(\chi_p, \gamma) v_x n_p \equiv \overline{W_{\mathrm{pl}}} v_x n_p. \tag{46}$$

The total current density of the particles averaged over the characteristic period of Larmor oscillations, $\tau_B = \varepsilon_p/B$, is

$$\mathbf{j} = 2 n_p \frac{\mathbf{B}}{B} v_B \sqrt{1 - v_x^2}, \tag{47}$$

with

$$v_B = v_B' \frac{2}{\pi} \frac{\arccos\left(v_x \sqrt{1 - v_x^2}\right)}{\sqrt{1 - v_x^2 (1 - v_x^2)}} \sim v_B'. \tag{48}$$

The factor 2 here arises from the fact that the electron and positron currents are co-directional. This comes from the observation that in the laboratory reference frame, the electric and magnetic fields are

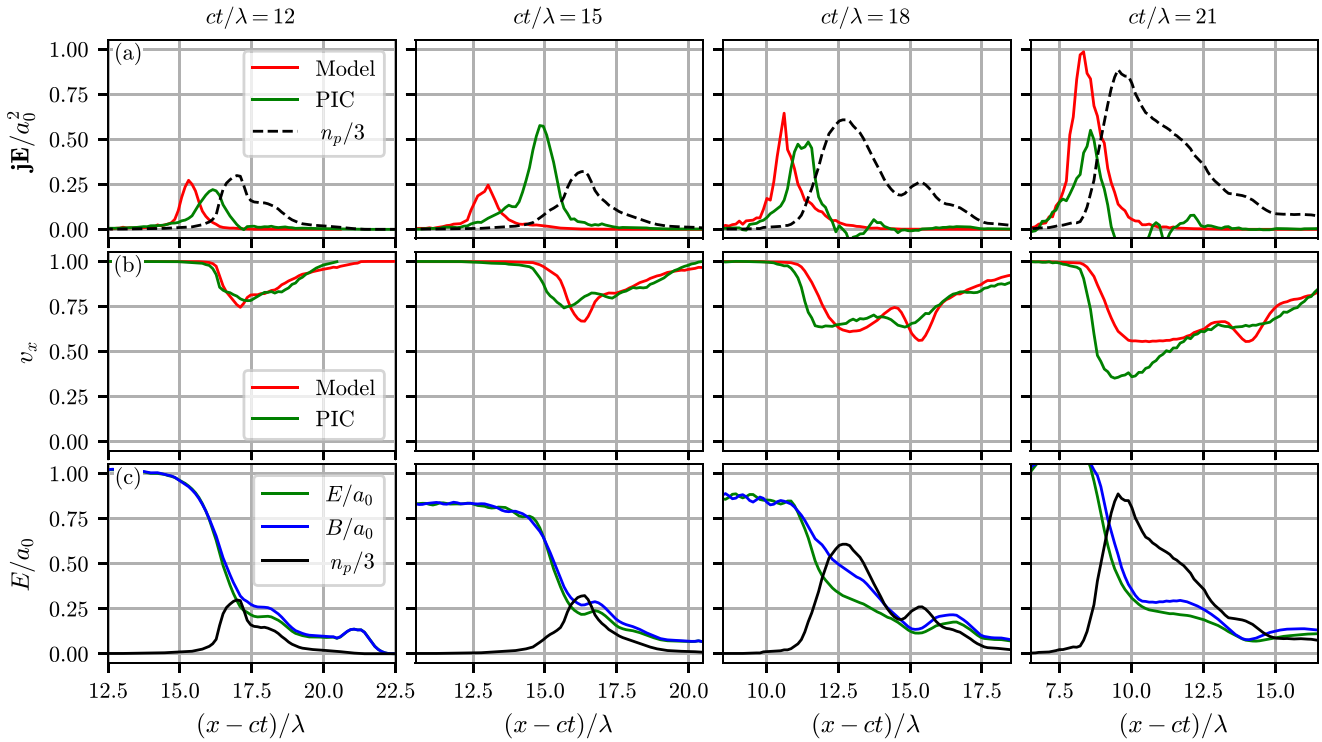

FIG. 4. Validation of the approximations used in the model. (a) Value of the product $\mathbf{j} \cdot \mathbf{E}$ computed from Eq. (35) and computed directly from the results of the QED-PIC simulations. (b) Mean longitudinal velocity of pairs computed from Eq. (49) and computed directly from the results of the QED-PIC simulations. (c) Distributions of electric field, magnetic field, and plasma density. Each plot is computed from the data averaged over a $\pm 2\lambda$ vicinity around the laser pulse axis in the yz plane.

©Author(s) 2021

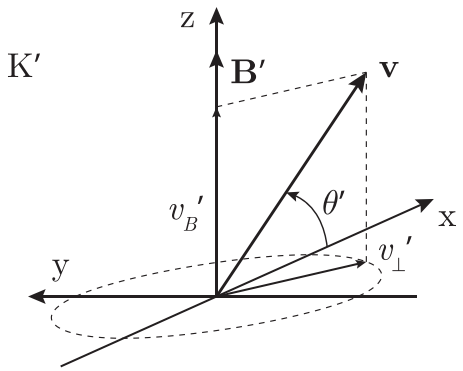

FIG. 5. Relation between the velocity vector and the magnetic field vector in the reference frame K' moving along the x axis with velocity $v_x = E/B$.

actually not exactly perpendicular, which means that in the reference frame K', there exists a small electric field directed along or opposite to the magnetic field (depending on the sign of the product $\mathbf{E}\cdot\mathbf{B}$). Consequently, the average electron velocity is in the opposite direction to that small electric field, and the average positron velocity is in the same direction as the field. This is not the case for the longitudinal motion of the pairs, which does not depend on the sign of the charge, and so the electron and positron currents cancel each other along the x axis but add together in the yz plane. This also suggests that the electron–positron plasma is actually a conducting media, and so some absorption of electromagnetic energy also occurs in that region, although it is significantly smaller than the absorption in the vacuum region that is seen in the QED-PIC simulations [see Fig. 4(a)], and therefore we do not take it into account in our model.

The value of v_B averaged over the particles, which we denote by ν, is the second fitting parameter of our model. We can roughly estimate it by noting that for a single particle the value of $v_B{}'$ cannot exceed its initial value during particle motion. The particles enter the plasma region after being accelerated by the laser pulse with predominantly longitudinal velocity, i.e., velocity along the x axis, and so the initial projection of the particle velocity onto the magnetic field, which lies in the yz plane, is small. Therefore, we expect our model to give valid results with values of ν closer to zero rather than to unity.

The electrodynamical behavior of the medium in response to the plane electromagnetic wave, involving the induction of a current along the magnetic field, is examined in Appendix B, and the main conclusion is that the ratio between the electric and magnetic fields in the medium can be expressed in terms of its density and the electric field amplitude as follows:

$$\frac{E}{B} = v_x = \sqrt{\frac{2}{1+\sqrt{1+(4n_p\nu/E)^2}}}. \tag{49}$$

The validity of this expression is verified by direct comparison against the mean values of the longitudinal velocity of the particles computed in the PIC simulation, as shown in Fig. 4(b).

III. MODEL FORMULATION AND COMPARISON WITH QED-PIC SIMULATIONS

The last remaining undefined terms are $\psi_{\rm vac}$ and $\psi_{\rm pl}$, which determine the vacuum and plasma regions, respectively, in space. We note that the longitudinal velocity v_x defined in Eq. (49) actually demarcates these regions: $v_x \approx 1$ in the vacuum region, and $v_x < 1$ in the plasma region. We therefore choose $\psi_{\rm vac}$ and $\psi_{\rm pl}$ in the following way:

$$\psi_{\rm vac} = v_x^M, \tag{50}$$

$$\psi_{\rm pl} = 1 - v_x^M, \tag{51}$$

where $M \sim 10$ is a constant. We choose the exact value of this parameter by defining the upper threshold for v_x above which we assume the plasma to be rarefied enough not to cause any collective effects. Therefore, we choose this threshold value to be 0.7 and $M = 8$.

The final set of cascade model equations is as follows:

$$\frac{\partial}{\partial t}n_p + \frac{\partial}{\partial x}(v_x n_p) = \overline{W_{\rm pair}}n_\gamma, \tag{52}$$

$$\frac{\partial}{\partial t}(\varepsilon_p n_p) + \frac{\partial}{\partial x}(v_p\varepsilon_p n_p) = \overline{W_{\rm pair}}n_\gamma\frac{\varepsilon_\gamma}{2} + \left(\mu E^{2/3}\varepsilon_\gamma^{1/3}\overline{G_{\rm rad}} - \overline{I_{\rm vac}}\right)n_\gamma\psi_{\rm vac} - \overline{I_{\rm pl}}n_p\psi_{\rm pl}, \tag{53}$$

$$\frac{\partial}{\partial t}n_\gamma + \frac{\partial}{\partial x}\left(\overline{v_{\gamma\parallel}}n_\gamma\right) = -\overline{W_{\rm pair}}n_\gamma + 2\overline{W_{\rm rad}}n_p\psi_{\rm pl}, \tag{54}$$

$$\frac{\partial}{\partial t}\left(\overline{v_{\gamma\parallel}}n_\gamma\right) + \frac{\partial}{\partial x}\left(\overline{v_{\gamma\parallel}^2}n_\gamma\right) = -\overline{V_{\rm pair}}n_\gamma + 2\overline{V_{\rm rad}}n_p\psi_{\rm pl}, \tag{55}$$

$$\frac{\partial}{\partial t}(\varepsilon_\gamma n_\gamma) + \frac{\partial}{\partial x}\left(\overline{v_{\gamma\parallel}}\varepsilon_\gamma n_\gamma\right) = -\overline{W_{\rm pair}}n_\gamma\varepsilon_\gamma + 2\overline{I_{\rm pl}}n_p\psi_{\rm pl}, \tag{56}$$

$$\frac{\partial}{\partial t}\left(\frac{E^2+E^2/v_x^2}{2}\right) + \frac{\partial}{\partial x}\left(\frac{E^2}{v_x}\right) = -2\mu E^{2/3}\varepsilon_\gamma^{1/3}\overline{G_{\rm rad}}n_\gamma\psi_{\rm vac}, \tag{57}$$

$$\frac{\partial}{\partial t}\Sigma_\gamma = \overline{I_{\rm vac}}n_\gamma\psi_{\rm vac}. \tag{58}$$

It is important to note that energy is conserved in the model, i.e.,

$$\int\left(2n_p\varepsilon_p + n_\gamma\varepsilon_\gamma + \frac{E^2+B^2}{2}\right)dx + \Sigma_\gamma = \text{const}. \tag{59}$$

Equations (52)–(57) were solved numerically using the method of lines (MOL): partial derivatives $\partial/\partial x$ were approximated with finite differences to derive a system of ODEs that was solved using the explicit Runge–Kutta method. This scheme is not internally conservative, and therefore the energy conservation was done manually at each integration step by clipping the derivative $\partial n_\gamma/\partial t$ so that the total energy did not grow. The relative error arising from this procedure turned out to be acceptably small. Fitting parameters were estimated manually by comparing the solution with the results of 3D QED-PIC

© Author(s) 2021

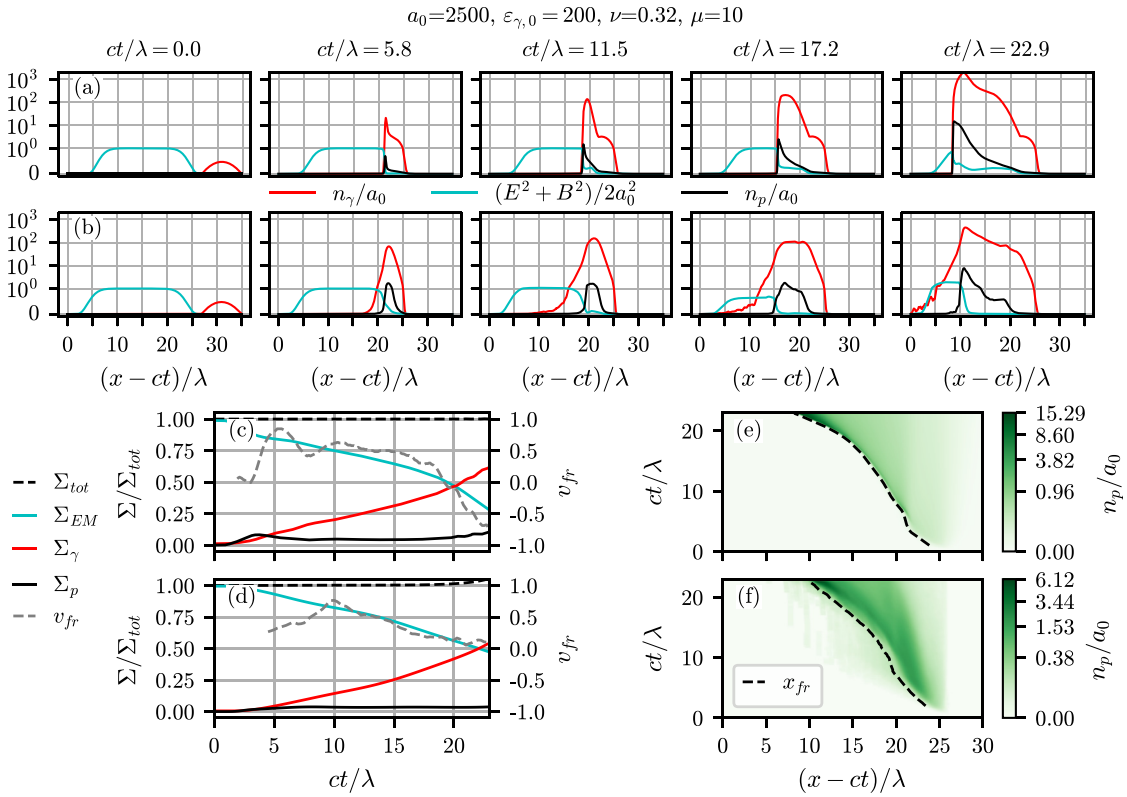

FIG. 6. Comparison between the solution of Eqs. (52)–(57) [(a), (c), and (e)] and the results of the QED-PIC simulations [(b), (d), and (f)] for laser amplitude a_0 = 2500 and $n_{\gamma,0} = 0.5a_0n_{cr}$. (a) and (b) Distributions of gamma-quantum density n_γ, electromagnetic energy density (E^2 + B^2)/2, and plasma density n_p at different time instants. Note that the scale of the vertical axis is linear in the range [0, 1] and logarithmic in the range [1, +∞]. (c) and (d) Energy balance: total energy of pairs Σ_p and of gamma quanta Σ_γ and electromagnetic energy Σ_{EM}, all normalized to the initial total energy of the system Σ_{tot}. The velocity of the plasma boundary v_{fr} is also plotted. (e) and (f) Distribution of pairs in the xt plane and the position of the plasma boundary x_{fr}. The numerical values of the fitting parameters used in the model solution are ν = 0.32 and μ = 10.

simulations based on two macroscopic properties, namely, the velocity of the cascade front and the energy balance. After testing the reduced model, it was found that there is a positive correlation between the parameter ν and the velocity of cascade front propagation. The parameter μ mostly determines the energy transfer from the laser to the cascade particles, and so the characteristic time of the laser energy depletion can be controlled by tweaking this parameter. Note that the estimated values of the fitting parameters are almost equal to each other for different initial conditions (see Figs. 6–8).

The 3D QED-PIC simulations were performed using the QUILL code,[42] which enables modeling of the QED effects via the Monte Carlo method. The initial distribution of the electromagnetic fields has the form of a plane wave with wavelength $\lambda = 2\pi c/\omega_L = 1$ μm and an amplitude a_0 propagating along the x axis with spatiotemporal envelope given by

$$a(x,y,z) = \cos^2\left(\frac{\pi}{2}\frac{x^4}{\sigma_x^4}\right)\cos^2\left[\frac{\pi}{2}\frac{(y^2+z^2)^2}{\sigma_r^4}\right]. \quad (60)$$

The transverse spatial size of the laser pulse is $2\sigma_r$ = 18 μm and the pulse duration is 60.5 fs ($2\sigma_x$ = 18.15 μm). The simulation box size is $30\lambda \times 30\lambda \times 30\lambda$ and the grid size is 3000 × 300 × 300. As discussed in Ref. 37, the final stage of QED cascade development in a single laser pulse is almost independent of the seed, and so we choose the seed in the form of a short gamma bunch counter-propagating to the laser pulse in order not to introduce into the interaction an electron–ion plasma that is significantly different from the forming electron–positron plasma. Such an initial seed can be incorporated into our model by initializing $v_{\gamma\|}(t=0) \approx -1$. The density distributions in our model and the PIC simulation coincide and are expressed by the formula $n_\gamma(t=0) = n_0 \max\{0, 1-(x-x_0)^2/w_\gamma^2\}$, where w_γ is the half-width of the bunch and x_0 is the position of its center. The initial energy of the gamma quanta was set to $200m_ec^2$.

Direct comparisons between the solutions of Eqs. (52)–(57) and the results of the QED-PIC simulations are shown in Figs. 6–8. The results from our model coincide with those of the full QED-PIC simulations qualitatively well in terms of the distributions of the particles and the electromagnetic field, as well as the energy balance. Also, we can clearly see the different regimes of cascade development in both cases.

The first regime is observed when a_0 of the laser pulse is not big enough or the gamma bunch is not dense enough. In this case, the

©Author(s) 2021

density of the produced electron–positron plasma does not reach the relativistic critical density such that $\nu_x \approx 1$, i.e., collective plasma effects do not occur. In this case, the plasma region is not present at all, and the newly born particles move in the unaltered field of the laser pulse, which is close to a plane wave. As discussed in Refs. 7 and 43–45, in this case the χ of the pairs does not grow during their motion in the plane wave. However, after each act of gamma-quantum emission, χ splits between the parent and child particles, and so, after a few generations, the χ of all the particles becomes negligibly small and therefore cascading ceases. Thus, for small enough a_0, the gamma quanta of the gamma bunch decay into pairs, leaving a "trail" of electrons and positrons, which are accelerated forward and co-propagate with the laser pulse. Although the density of the plasma is small, the total number of pairs can be large enough that a significant portion of the laser energy is transferred to them [see Figs. 8(c) and 8(d)]. Because in this regime all the particles propagate independently from each other, the cascade front propagates with almost constant velocity $v_{\rm fr} \approx -0.5$.

In the second regime, the cascade develops as discussed in Sec. I. The peak of the pair density propagates toward the laser with a much slower velocity (relative to the leading edge of the laser pulse) than in the first regime. Moreover, the density of the plasma grows in time, in contrast to the first regime, where the plasma density at each point stays almost the same after the initial gamma bunch passes that point. In fact, as mentioned in Sec. II E, the dense electron–positron plasma almost does not absorb the laser field, which is why, although in this regime the total number of pairs is much larger than in the first regime, the rates of energy transfer from the electromagnetic field to the pairs are similar in the two regimes.

If a_0 lies in between the values at which either the first or the second regime is observed, then, during its initial stage, the cascade resembles an S-type cascade, which is clearly indicated by the negative value of the velocity of the cascade front [see the gray dashed lines in Figs. 7(c) and 7(d)]. At some point, the density of pairs becomes large enough to alter the laser propagation and to shift the cascade dynamics to the self-sustained regime. The change between these two regimes is indicated by an abrupt change in the velocity of the cascade front. The initial stage (the stage of an S-type cascade) can also be seen for larger values of a_0 (see Fig. 6), although it is much shorter and is barely noticeable in the results of the QED-PIC simulations.

We have also verified the results of the simplified model developed by us in Ref. 37, from which a relation between the mean longitudinal velocity of the cascade particles and the cascade front velocity was obtained. This model prediction, calculated on the basis of the mean velocity of the cascade particles, roughly coincides with the actual velocity observed in the model solution (see Fig. 9) at the stage of cascade self-sustenance. As this stage never starts for $a_0 = 1000$, this simplified model cannot be applied in that case.

There are some features that are not captured by our model and that are worth noting. First, in the PIC simulation, there is a distinct

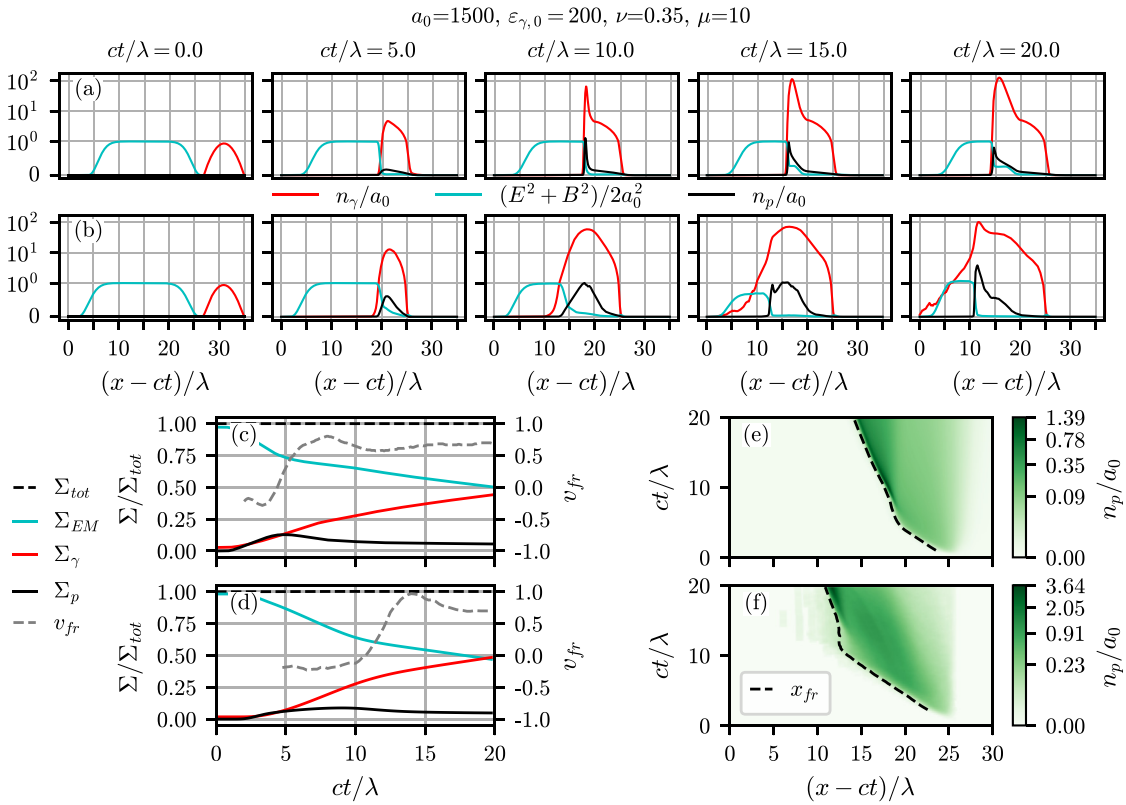

FIG. 7. Same as Fig. 6, but for $a_0 = 1500$ and $n_{\gamma,0} = a_0 n_{\rm cr}$. The values of the fitting parameters are $\nu = 0.35$ and $\mu = 10$.

©Author(s) 2021

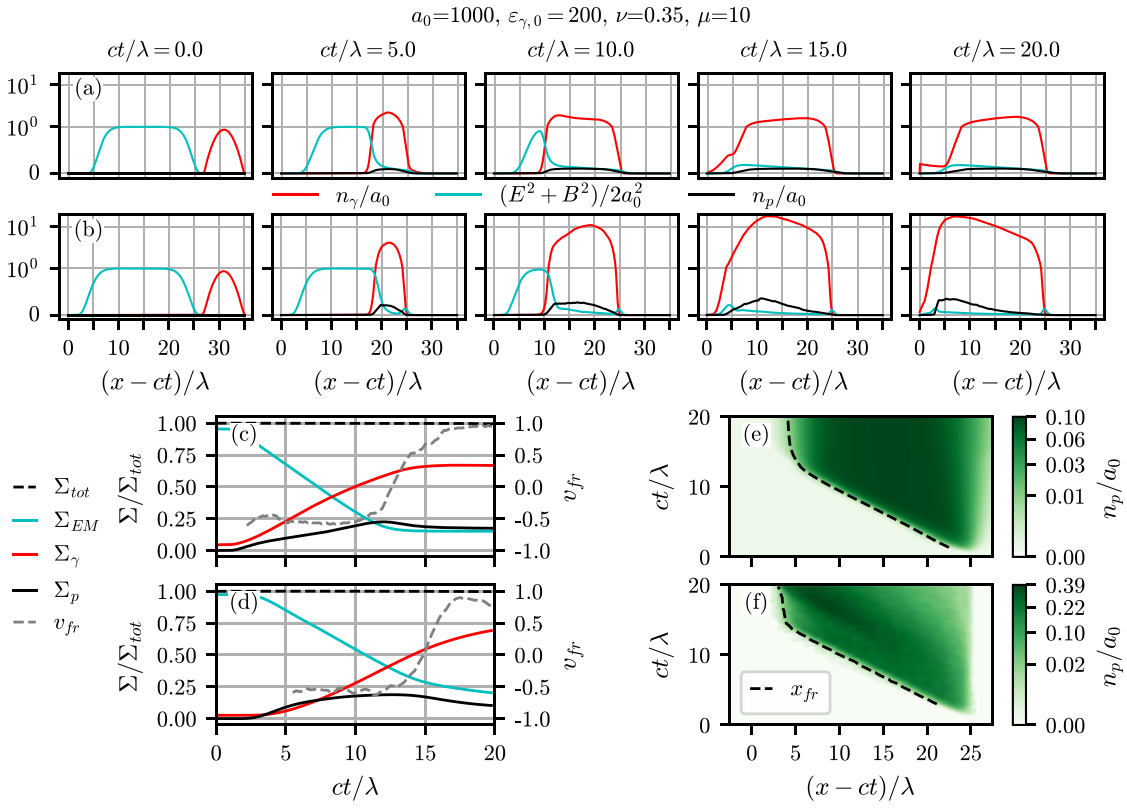

FIG. 8. Same as Fig. 6, but for a_0 = 1000 and $n_{\gamma,0} = a_0 n_{cr}$. The values of the fitting parameters are ν = 0.35 and μ = 10.

tail of the gamma-quanta spatial distribution counter-propagating to the laser pulse. These gamma quanta have relatively low energy and thus are unable to photoproduce pairs. Our model predicts that the edges of the plasma and gamma-quanta distributions coincide almost exactly. The total energy carried away by this sort of gamma quanta is insignificant, and so this feature is not crucial for cascade development. The reason why our model cannot capture this feature is that we assume the distribution functions to be monoenergetic. Higher accuracy could be obtained if we were to split the gamma quanta into several groups with different energies and describe them separately, and this feature would then be present in our solutions. However, as already mentioned in Sec. II, this modification would greatly complicate the model without leading to significant qualitative changes in the solutions. Second, both the total number of pairs and the peak plasma density are larger in the QED-PIC simulation than in our model solution for smaller values of a_0. One of the reasons behind these discrepancies is that our model is one-dimensional and thus does not describe laser pulse diffraction. In the 3D-PIC simulations, the simulation box is always limited, and so a pure plane wave cannot be achieved in the simulations. As a consequence, the envelope of the laser pulse evolves such that the magnitude of the laser pulse in the vacuum region may differ from its initial value a_0 [see Fig. 4(c)]. An increase in effective laser pulse intensity generally leads to an increase in the probabilities of QED processes and thus to more abundant pair photoproduction. The net effect of the inconstancy of the laser pulse intensity can be partially accounted for by choosing the value of a_0 in the model solution to be larger than the value initially set in the PIC simulation.

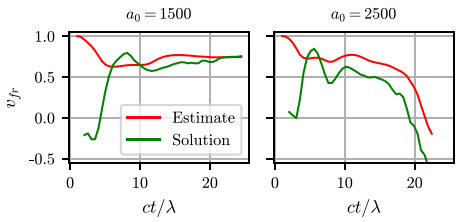

FIG. 9. Velocity of the cascade front observed in the model solution (green line) and obtained from the simplified model developed in Ref. 37 (red line) calculated from the mean velocity of the particles located at a depth of 2λ behind the cascade front.

IV. CONCLUSION

We have developed a self-consistent model of QED cascade development in an extremely intense laser pulse. The complete description of that interaction requires solution of Maxwell's equations along with the kinetic equations for electrons, positrons, and gamma photons. This system of equations is too complex for analytical

©Author(s) 2021

methods and is usually solved numerically with QED-PIC codes that consume a lot of computational resources. To derive the reduced equations for a computationally light model, we adopt some assumptions, the main ones being quasi-one-dimensional hydrodynamics, a locally quasi-monoenergetic distribution function for the particles, and a plane wave approximation for the laser radiation. The simplified system of equations thereby derived is written in closed form and is solved numerically. Despite the complexity and nonlinearity of the cascade dynamics, it turns out that a relatively simple one-dimensional model can qualitatively predict cascade development, for example, the macroscopic spatiotemporal distribution of particles and the energy balance in the system. This justifies the analytical reasoning behind the model and hence our understanding of the phenomena involved. Although there are several discrepancies between the predictions of our model and the results of QED-PIC simulations, the reasons behind these have been identified, and for some the methods by which they can be resolved have been discussed.

We stress that our model is suitable for a complete description of QED cascade development in a single laser pulse. For example, various regimes of the interaction based on the intensity of the laser pulse are revealed by both full QED-PIC simulations and our model.

We believe that our model can also be adapted to explore regimes of QED cascades in different environments: laser interaction with targets, including foils, particle beams, and gamma quanta, beam–beam interaction, etc. Therefore, further extensive tests of the model are planned to be carried out in the future.

SUPPLEMENTARY MATERIAL

See the supplementary material for animated visualizations of positron tracks, cascade development, and the 3D QED-PIC simulation.

ACKNOWLEDGMENTS

This research was supported by the Russian Science Foundation (Grant No. 20-12-00077) (PIC simulations, development of the analytical model, numerical scheme, and numerical solution of the model equations), and the Foundation for the Advancement of Theoretical Physics and Mathematics "BASIS" (Grant No. 19-1-5-10-1) (comparison to the simplified model developed in Ref. 37).

APPENDIX A: PARTICLE ACCELERATION IN A PLANE WAVE

Let us consider a single electron moving in the field of a plane circularly polarized electromagnetic wave.[46,47] The vector potential of the wave is chosen as

$$\mathbf{A} = a_0\,(\mathbf{e}_y \cos\xi + \mathbf{e}_z \sin\xi), \tag{A1}$$

$$\xi = t - x. \tag{A2}$$

The Hamiltonian of the problem is

$$H = \sqrt{1 + (\mathscr{P} + \mathbf{A})^2}, \tag{A3}$$

where $\mathscr{P} = \mathbf{p} - \mathbf{A}$ is the generalized momentum of the electron with momentum $\mathbf{p}$. For the equations of motion, we get

$$\frac{d\mathcal{P}_y}{dt} = -\frac{\partial H}{\partial y} = 0, \tag{A4}$$

$$\frac{d\mathcal{P}_z}{dt} = -\frac{\partial H}{\partial z} = 0, \tag{A5}$$

$$\frac{d\mathcal{P}_x}{dt} = \frac{dp_x}{dt} = -\frac{\partial H}{\partial x} = \frac{\partial H}{\partial \xi}, \tag{A6}$$

$$\frac{d\varepsilon}{dt} = \frac{dH}{dt} = \frac{\partial H}{\partial t} + \cancel{[H\mathcal{P}]^0} = \frac{\partial H}{\partial \xi}. \tag{A7}$$

From these equations, we find that

$$p_y + A_y = \text{const}, \tag{A8}$$

$$p_z + A_z = \text{const}, \tag{A9}$$

$$p_x - \varepsilon = \text{const}. \tag{A10}$$

Let us define the initial conditions for the electron:

$$p_x\,(t = t_0) = p_0 \cos\theta, \tag{A11}$$

$$p_y\,(t = t_0) = p_0 \sin\theta, \tag{A12}$$

$$p_z\,(t = t_0) = 0, \tag{A13}$$

$$x\,(t = t_0) = x_0, \tag{A14}$$

$$\xi\,(t = t_0) \equiv t_0 - x_0, \tag{A15}$$

$$\varepsilon_0 \equiv \sqrt{1 + p_0^2}. \tag{A16}$$

We can then rewrite Eqs. (A8)–(A10) as

$$p_y = p_0 \sin\theta + a_0\,(\cos\xi_0 - \cos\xi), \tag{A17}$$

$$p_z = a_0\,(\sin\xi_0 - \sin\xi), \tag{A18}$$

$$\varepsilon = p_x + \rho_0, \tag{A19}$$

$$\rho_0 = \varepsilon_0 - p_0 \cos\theta. \tag{A20}$$

Equation (A3) can be rewritten in the form

$$\varepsilon = \sqrt{1 + p_x^2 + p_y^2 + p_z^2}. \tag{A21}$$

Combining Eqs. (A19)–(A21), we get the following equation for ε:

$$\varepsilon = \{\varepsilon^2 - 1 - a_0^2\,(\sin\xi - \sin\xi_0)^2 - [p_0 \sin\theta + a_0\,(\cos\xi - \cos\xi_0)]^2\}^{1/2} + \rho_0. \tag{A22}$$

The energy gain $\Delta\varepsilon = \varepsilon - \varepsilon_0$ can be found analytically as

$$\Delta\varepsilon = \frac{2a_0 p_0}{\rho_0} \sin\frac{\Delta\xi}{2}\left(\frac{a_0}{p_0}\sin\frac{\Delta\xi}{2} - \sin\theta \sin\frac{\xi + \xi_0}{2}\right), \tag{A23}$$

where ξ is the current phase of the electron. If we assume that $1 \ll p_0 \ll a_0$, then the second term in parentheses in Eq. (A23) is insignificant for any ξ and ξ_0 compared with the first term, and so we can omit it. Another reason why we can ignore the second term is the fact that it depends on the absolute phase of the particle and thus its value averaged over the wave period is equal to zero. We therefore have

© Author(s) 2021

$$\Delta\varepsilon \approx \frac{2a_0^2}{\rho_0}\sin^2\left(\frac{\Delta\xi}{2}\right). \tag{A24}$$

Next, we calculate $\Delta\xi$. We have

$$\frac{d\xi}{dx} = \frac{d}{dx}(t-x) = \frac{1}{v_x} - 1 = \frac{\varepsilon}{p_x} - 1 = \frac{\varepsilon - p_x}{p_x} = \frac{\rho_0}{p_x} \tag{A25}$$

and

$$\Delta x\rho_0 = \int_{\xi_0}^{\xi_0+\Delta\xi} p_x\, d\xi = \int_{\xi_0}^{\xi_0+\Delta\xi} (\Delta\varepsilon + p_0\cos\theta)\, d\xi = \frac{a_0^2}{\rho_0}(\Delta\xi - \sin\Delta\xi) + p_0\cos\theta\Delta\xi. \tag{A26}$$

If we assume again that $a_0 \gg p_0$, then Eq. (A26) can be rewritten as

$$\Delta\xi - \sin\Delta\xi = \frac{\rho_0^2}{a_0^2}\Delta x. \tag{A27}$$

Note that $\rho_0 < p_0 \ll a_0$ and that Δx is the distance along the x axis between the initial and final positions of the electron. In the case of our cascade model, the initial position coincides with the position of the parent gamma quantum decay, and the final position is the position of the cascade front. QED-PIC simulations show that the distance Δx does not exceed several λ, which in dimensionless variables means that $\Delta x/2\pi \sim 1$. Therefore, in Eq. (A27), we can assume that $\Delta\xi \ll 1$ and leave only the first nonvanishing term in the left-hand side expansion:

$$\frac{\Delta\xi^3}{6} \approx \frac{\rho_0^2}{a_0^2}\Delta x, \tag{A28}$$

$$\Delta\xi \approx \left(6\Delta x\frac{\rho_0^2}{a_0^2}\right)^{1/3}. \tag{A29}$$

Substituting this solution into Eq. (A24), we get

$$\Delta\varepsilon \equiv \Delta\varepsilon_{\rm acc} \approx \left[\frac{9}{2}a_0^2\varepsilon_0\Delta x^2(1-\cos\theta)\right]^{1/3}, \tag{A30}$$

where we have also assumed that $\rho_0 \approx \varepsilon_0(1-\cos\theta)$. The duration of particle motion can be also calculated to be

$$\Delta\xi = \Delta t - \Delta x, \tag{A31}$$

and under the assumption that $\Delta\xi \ll \Delta x$, which follows from the assumption $p_0 \ll a_0$, we find that $\Delta x \approx \Delta t$. This is an obvious conclusion, because, under our assumptions, the particle can be considered ultrarelativistic and its velocity along the x axis to be close to the speed of light.

We now estimate the radiative losses during particle motion in a plane wave. The governing parameter χ in the plane wave is calculated as follows:

$$\chi = \frac{\varepsilon}{\mathcal{E}_S}\sqrt{(\mathbf{E}+\mathbf{v}\times\mathbf{B})^2 - (\mathbf{v}\cdot\mathbf{E})^2} = \frac{a_0}{\mathcal{E}_S}(\varepsilon - p_x), \tag{A32}$$

where $\mathbf{E} = -\partial\mathbf{A}/\partial t = a_0(-\mathbf{e}_y\sin\xi + \mathbf{e}_z\cos\xi)$ is the electric field and $\mathbf{B} = \nabla\times\mathbf{A} = a_0(-\mathbf{e}_y\cos\xi + \mathbf{e}_z\sin\xi)$ is the magnetic field. It can be seen from Eqs. (A10) and (A32) that in the classical approach, χ is constant during particle motion. If we take account of QED effects, then the parameter χ changes after each act of gamma-quantum radiation. Although this process can be considered instantaneous, for the sake of estimating the energy loss it is convenient to introduce a continuous force of radiation friction F_{rr}:

$$\frac{d\varepsilon}{dt} = -\mathbf{v}\cdot\mathbf{E} - F_{rr}v^2, \tag{A33}$$

$$\frac{dp_x}{dt} = -(\mathbf{v}\times\mathbf{B})_x - F_{rr}v_x, \tag{A34}$$

$$\frac{d\mathbf{v}}{dt} = -\frac{1}{\varepsilon}\left[\mathbf{E} - \mathbf{v}(\mathbf{v}\cdot\mathbf{E}) + \mathbf{v}\times\mathbf{B} + \frac{F_{rr}}{\varepsilon^2}\mathbf{v}\right]. \tag{A35}$$

If we assume the particle to be ultrarelativistic, then Eq. (A35) does not depend explicitly on the radiative losses, since $F_{rr}/\varepsilon^2 \ll 1$. Owing to radiative losses, ε changes differently in time compared with the case in which such losses are absent, but we will assume that the equality $\mathbf{v}\cdot\mathbf{E} = (\mathbf{v}\times\mathbf{B})_x$, which follows from the conservation of $\gamma - p_x$, still holds. Then, the equation for χ can be significantly simplified:

$$\frac{d\chi}{dt} = \frac{a_0}{\mathcal{E}_S}\left(\frac{d\varepsilon}{dt} - \frac{dp_x}{dt}\right) \approx -\frac{a_0}{\mathcal{E}_S}(v^2 - v_x)F_{rr} \approx -\frac{a_0}{\mathcal{E}_S}(1-v_x)F_{rr}, \tag{A36}$$

with $F_{rr} \equiv I_{\rm rad}(\chi)$, where $I_{\rm rad}$ is defined in Eq. (10) and an expression for it can be found, for example, in Ref. 18. We assume again that the term v_x can be calculated according to the classical approach without accounting for radiative losses, i.e.,

$$1 - v_x = 1 - \frac{p_x}{\varepsilon} = \frac{\varepsilon - p_x}{\varepsilon} = \frac{\rho_0}{\varepsilon} = \frac{\rho_0}{\varepsilon_0 + \left(\frac{9}{2}a_0^2\rho_0 t^2\right)^{1/3}}. \tag{A37}$$

So, finally,

$$\frac{d\chi}{dt} = -\frac{\chi_0 I_{\rm rad}(\chi)}{\varepsilon_0 + \left(\frac{9}{2}a_0^2\rho_0 t^2\right)^{1/3}}. \tag{A38}$$

The total energy loss due to radiation is then calculated as follows:

$$\Delta\varepsilon_{\rm rad} = \int_0^{\Delta t} I_{\rm rad}(\chi(t))\, dt \approx \int_0^{\Delta x} I_{\rm rad}(\chi(t))\, dt. \tag{A39}$$

The values of $\Delta\varepsilon_{\rm acc}$ and $\Delta\varepsilon_{\rm rad}$ obtained using this approach overestimate the corresponding values calculated numerically from the solution of the particle equations of motion taking account of radiation friction [Eqs. (A33) and (A35)], although the order of magnitude is estimated correctly. In the cascade model, the value Δx is unknown, because it is the distance along the x axis between the position of particle birth and the position where the particle crosses the moving cascade front. This quantity cannot be calculated in our model. Also, we are interested only in the total energy change during the time the particle stays in the vacuum region, and so the exact dependence of particle energy on time is irrelevant. Thus, we calculate the values $\Delta\varepsilon_{\rm acc}$ and $\Delta\varepsilon_{\rm rad}$ as follows:

$$\Delta\varepsilon_{\rm acc} = \mu 2^{1/3}a_0^{2/3}\varepsilon_0^{1/3}(1-\cos\theta)^{1/3}, \tag{A40}$$

$$\Delta\varepsilon_{\rm rad} = \int_0^{\sqrt{4\mu^3/9}} I_{\rm rad}(\chi)\, dt, \tag{A41}$$

© Author(s) 2021

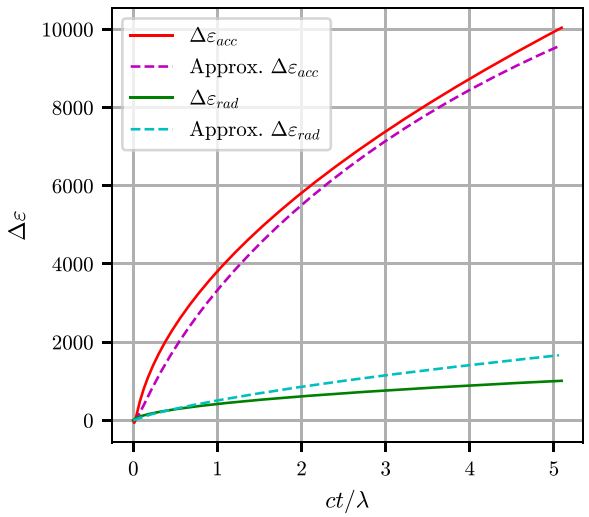

FIG. 10. Validation of the approximations used to describe the energy gain due to acceleration and the energy loss due to gamma-quantum emission by a single particle in a plane wave for $a_0 = 2500$, $p_0 = 500$, and $\theta = \pi$. The solid lines correspond to the numerical solution of Eqs. (A33)–(A35) and the dashed lines to the approximations (A40) and (A41), where $\mu = ct/3\lambda$.

with

$$\frac{d\chi}{dt} = -\frac{\chi_0 I_{\rm rad}(\chi)}{\varepsilon_0 + \left[\frac{9}{2}a_0^2\varepsilon_0 t^2(1-\cos\theta)\right]^{1/3}}, \tag{A42}$$

where μ is a fitting parameter that determines the characteristic time spent by the particle in the vacuum region. We set this parameter equally for all the particles. It turns out that by tuning this parameter, the values of both $\Delta\varepsilon_{\rm acc}$ and $\Delta\varepsilon_{\rm rad}$ can be estimated with good accuracy (see Fig. 10).

APPENDIX B: EFFECTIVE DIELECTRIC PERMITTIVITY OF THE e^+e^- PLASMA

Let us consider the propagation of a circularly polarized plane electromagnetic wave along the x axis inside a medium that is inhomogeneous along the x axis, which induces a current $\mathbf{j} = 2n_p\mathbf{v}$. Maxwell's equations then take the form

$$\frac{\partial E_z}{\partial x} = \frac{\partial B_y}{\partial t}, \tag{B1}$$

$$\frac{\partial E_y}{\partial x} = -\frac{\partial B_z}{\partial t}, \tag{B2}$$

$$\frac{\partial B_z}{\partial x} = -\frac{\partial E_y}{\partial t} - 2n_p v_y, \tag{B3}$$

$$\frac{\partial B_y}{\partial x} = \frac{\partial E_z}{\partial t} + 2n_p v_z. \tag{B4}$$

It is convenient to introduce the following complex variables:

$$\epsilon = E_y + iE_z, \tag{B5}$$

$$\beta = B_z - iB_y, \tag{B6}$$

$$v_y + iv_z = \frac{\epsilon}{|\epsilon|}(v_E + iv_{E\perp}), \tag{B7}$$

where v_E and $v_{E\perp}$ are the plasma velocities along and across the electric field, respectively. We can also introduce the vector potential a as follows:

$$\epsilon = -\frac{\partial a}{\partial t}, \qquad \beta = \frac{\partial a}{\partial x}. \tag{B8}$$

As a result, Eqs. (B1)–(B4) can be rewritten in the form

$$\frac{\partial^2 a}{\partial x^2} = \frac{\partial^2 a}{\partial t^2} - 2n_p\frac{\partial a}{\partial t}\left|\frac{\partial a}{\partial t}\right|^{-1}(\bar{v}_E + i\bar{v}_{E\perp}). \tag{B9}$$

We seek a solution in the form of a plane monochromatic wave with variable amplitude:

$$a = E(x)e^{i\int^x \kappa(x)\,dx - it}, \tag{B10}$$

where both $E(x)$ and $\kappa(x)$ are real functions and $E(x)$ is the amplitude of the electric field. The final form of the equations is

$$\frac{\partial^2 E}{\partial x^2} + E(1-\kappa^2) + 2n_p v_{E\perp} = 0, \tag{B11}$$

$$E\frac{\partial \kappa}{\partial x} + 2\kappa\frac{\partial E}{\partial x} - 2n_p v_E = 0. \tag{B12}$$

If the plasma is slightly inhomogeneous, then we can apply the WKB approximation to solve the problem. If the plasma density distribution has the form of an inhomogeneous slab (as in the case of cascade development), then this approximation is valid inside the plasma but may be invalid near the edges. Assuming that the scale of plasma inhomogeneity L is larger than the laser wavelength λ, we can neglect the term with the second derivative: $\partial^2 E/\partial x^2 \sim E/L^2 \ll k^2 E = (2\pi)^2 E/\lambda^2$. So,

$$E(1-\kappa^2) + 2n_p v_{E\perp} = 0. \tag{B13}$$

Solving this equation, we get

$$\kappa \equiv \frac{B}{E} = \sqrt{1 + \frac{2n_p v_\perp}{E}}, \tag{B14}$$

where we have $v_\perp^2 = v_E^2 + v_{E\perp}^2 = v_y^2 + v_z^2$. We specify the expression $v_\perp$ as follows [see Eq. (47)]:

$$v_\perp = v\sqrt{1 - v_x^2}. \tag{B15}$$

Note that in the case $v > 0$, according to Eq. (B14), $B > E$, and thus $1/\kappa$ has the meaning of the drift velocity v_x, and so

$$\frac{1}{v_x} = \sqrt{1 + \frac{2n_p v}{E}\sqrt{1 - v_x^2}}. \tag{B16}$$

The solution of this equation is[37]

$$v_x = \sqrt{\frac{2}{1 + \sqrt{1 + S^2}}}, \tag{B17}$$

©Author(s) 2021

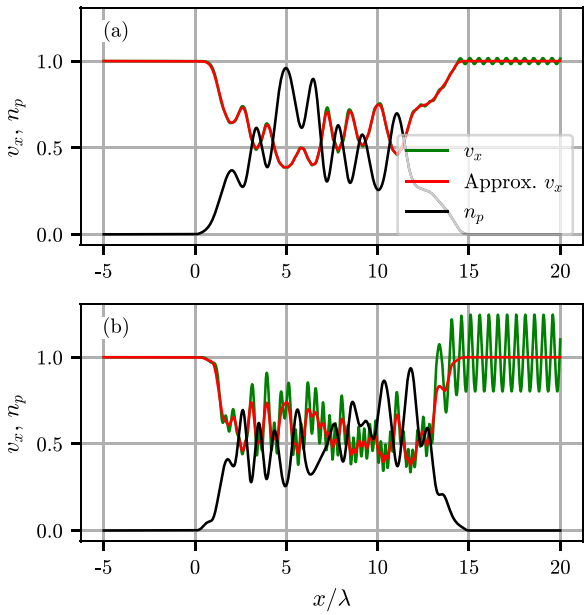

FIG. 11. Longitudinal velocity v_x computed by numerical solution of Eqs. (B11) and (B12) (green line) and from the approximate expression (B17) (red line) for the plasma density in the form of an inhomogeneous slab (black line). In (a), the scale of inhomogeneity is smaller than the wavelength, and hence the WKB approximation is valid, while in (b), the scale of inhomogeneity is larger than the wavelength.

$$S = \frac{4n_p\nu}{E}. \tag{B18}$$

A comparison of this approximate expression with the exact numerical solution of Eqs. (B11) and (B12) is shown in Fig. 11 both for the case in which the WKB approximation is valid and for the case in which it is not.

Since $\nu^2 = 1$ is assumed in the derivation of Eq. (B17), this equation is valid for any reference frame in which particles are ultrarelativistic, for example, the laboratory reference frame.

REFERENCES

[1]P. A. Sturrock, "A model of pulsars," Astrophys. J. **164**, 529 (1971).

[2]J. K. Daugherty and A. K. Harding, "Electromagnetic cascades in pulsars," Astrophys. J. **252**, 337–347 (1982).

[3]E. N. Nerush and I. Yu. Kostyukov, "Radiation emission by extreme relativistic electrons and pair production by hard photons in a strong plasma wakefield," Phys. Rev. E **75**, 057401 (2007).

[4]A. R. Bell and J. G. Kirk, "Possibility of prolific pair production with high-power lasers," Phys. Rev. Lett. **101**, 200403 (2008).

[5]E. N. Nerush, I. Yu. Kostyukov, A. M. Fedotov, N. B. Narozhny, N. V. Elkina, and H. Ruhl, "Laser field absorption in self-generated electron-positron pair plasma," Phys. Rev. Lett. **106**, 035001 (2011).

[6]C. P. Ridgers, C. S. Brady, R. Duclous, J. G. Kirk, K. Bennett, T. D. Arber, A. P. L. Robinson, and A. R. Bell, "Dense electron-positron plasmas and ultraintense γ rays from laser-irradiated solids," Phys. Rev. Lett. **108**, 165006 (2012).

[7]N. B. Narozhny and A. M. Fedotov, "Quantum-electrodynamic cascades in intense laser fields," Phys.-Usp. **58**, 95 (2015).

[8]I. Yu. Kostyukov and E. N. Nerush, "Production and dynamics of positrons in ultrahigh intensity laser-foil interactions," Phys. Plasmas **23**, 093119 (2016).

[9]E. N. Nerush, D. A. Serebryakov, and I. Yu. Kostyukov, "Weibel instability in hot plasma flows with the production of gamma-rays and electron–positron pairs," Astrophys. J. **851**, 129 (2017).

[10]E. S. Efimenko, A. V. Bashinov, A. A. Gonoskov, S. I. Bastrakov, A. A. Muraviev, I. B. Meyerov, A. V. Kim, and A. M. Sergeev, "Laser-driven plasma pinching in e^-e^+ cascade," Phys. Rev. E **99**, 031201 (2019).

[11]V. Yakimenko, S. Meuren, F. Del Gaudio, C. Baumann, A. Fedotov, F. Fiuza, T. Grismayer, M. Hogan, A. Pukhov, L. Silva *et al.*, "Prospect of studying nonperturbative QED with beam-beam collisions," Phys. Rev. Lett. **122**, 190404 (2019).

[12]H. J. Bhabha and W. Heitler, "The passage of fast electrons and the theory of cosmic showers," Proc. R. Soc. London, Ser. A **159**, 432–458 (1937).

[13]M. A. Ruderman and P. G. Sutherland, "Theory of pulsars-polar caps, sparks, and coherent microwave radiation," Astrophys. J. **196**, 51–72 (1975).

[14]P. Mészáros, "Gamma-ray bursts," Rep. Prog. Phys. **69**, 2259 (2006).

[15]Y. B. Zel'dovich, "Interaction of free electrons with electromagnetic radiation," Sov. Phys. Usp. **18**, 79 (1975).

[16]F. Rohrlich, *Classical Charged Particles* (World Scientific Publishing Company, 2007).

[17]V. I. Ritus, "Quantum effects of the interaction of elementary particles with an intense electromagnetic field," J. Sov. Laser Res. **6**, 497–617 (1985).

[18]V. N. Baier, V. M. Katkov, and V. M. Strakhovenko, *Electromagnetic Processes at High Energies in Oriented Single Crystals* (World Scientific, 1998).

[19]See http://www.eli-laser.eu for the extreme light infrastructure (ELI).

[20]See https://portail.polytechnique.edu/luli/en/cilex-apollon/apollon for APOLLON.

[21]A. Gonoskov, I. Gonoskov, C. Harvey, A. Ilderton, A. Kim, M. Marklund, G. Mourou, and A. Sergeev, "Probing nonperturbative QED with optimally focused laser pulses," Phys. Rev. Lett. **111**, 060404 (2013).

[22]E. G. Gelfer, A. A. Mironov, A. M. Fedotov, V. F. Bashmakov, E. N. Nerush, I. Yu. Kostyukov, and N. B. Narozhny, "Optimized multibeam configuration for observation of QED cascades," Phys. Rev. A **92**, 022113 (2015).

[23]T. Grismayer, M. Vranic, J. L. Martins, R. A. Fonseca, and L. O. Silva, "Laser absorption via quantum electrodynamics cascades in counter propagating laser pulses," Phys. Plasmas **23**, 056706 (2016).

[24]T. Grismayer, M. Vranic, J. L. Martins, R. A. Fonseca, and L. O. Silva, "Seeded QED cascades in counterpropagating laser pulses," Phys. Rev. E **95**, 023210 (2017).

[25]M. Jirka, O. Klimo, M. Vranic, S. Weber, and G. Korn, "QED cascade with 10 PW-class lasers," Sci. Rep. **7**, 15302 (2017).

[26]W. Luo, W.-Y. Liu, T. Yuan, M. Chen, J.-Y. Yu, F.-Y. Li, D. Del Sorbo, C. Ridgers, and Z.-M. Sheng, "QED cascade saturation in extreme high fields," Sci. Rep. **8**, 8400 (2018).

[27]P. Zhang, S. S. Bulanov, D. Seipt, A. V. Arefiev, and A. G. R. Thomas, "Relativistic plasma physics in supercritical fields," Phys. Plasmas **27**, 050601 (2020).

[28]E. N. Nerush, V. F. Bashmakov, and I. Yu. Kostyukov, "Analytical model for electromagnetic cascades in rotating electric field," Phys. Plasmas **18**, 083107 (2011).

[29]D. Del Sorbo, D. R. Blackman, R. Capdessus, K. Small, C. Slade-Lowther, W. Luo, M. J. Duff, A. P. L. Robinson, P. McKenna, Z.-M. Sheng *et al.*, "Efficient ion acceleration and dense electron–positron plasma creation in ultra-high intensity laser-solid interactions," New J. Phys. **20**, 033014 (2018).

[30]I. Yu. Kostyukov, I. I. Artemenko, and E. N. Nerush, "Growth rate of QED cascades in a rotating electric field," **2018**, 259–263.

[31]T. Yuan, J. Y. Yu, W. Y. Liu, S. M. Weng, X. H. Yuan, W. Luo, M. Chen, Z. M. Sheng, and J. Zhang, "Spatiotemporal distributions of pair production and cascade in solid targets irradiated by ultra-relativistic lasers with different polarizations," Plasma Phys. Controlled Fusion **60**, 065003 (2018).

[32]W. Luo, S.-D. Wu, W.-Y. Liu, Y.-Y. Ma, F.-Y. Li, T. Yuan, J.-Y. Yu, M. Chen, and Z.-M. Sheng, "Enhanced electron-positron pair production by two obliquely incident lasers interacting with a solid target," Plasma Phys. Controlled Fusion **60**, 095006 (2018).

[33]Y. Lu, T.-P. Yu, L.-X. Hu, Z.-Y. Ge, W.-Q. Wang, J.-X. Liu, K. Liu, Y. Yin, and F.-Q. Shao, "Enhanced copious electron–positron pair production via electron

©Author(s) 2021

injection from a mass-limited foil," Plasma Phys. Controlled Fusion **60**, 125008 (2018).

[34]B. Martinez, M. Lobet, R. Duclous, E. d'Humières, and L. Gremillet, "High-energy radiation and pair production by Coulomb processes in particle-in-cell simulations," Phys. Plasmas **26**, 103109 (2019).

[35]V. B. Berestetskii, E. M. Lifshitz, and L. P. Pitaevskii, *Quantum Electrodynamics* (Butterworth-Heinemann, 1982), Vol. 4.

[36]A. A. Mironov, N. B. Narozhny, and A. M. Fedotov, "Collapse and revival of electromagnetic cascades in focused intense laser pulses," Phys. Lett. A **378**, 3254–3257 (2014).

[37]A. S. Samsonov, E. N. Nerush, and I. Yu. Kostyukov, "Laser-driven vacuum breakdown waves," Sci. Rep. **9**, 11133 (2019).

[38]V. E. Semenov, "Breakdown wave in the self-consistent field of an electromagnetic wave beam," Sov. J. Plasma Phys. **8**, 347–350 (1982).

[39]J. G. Kirk, A. R. Bell, and C. P. Ridgers, "Pair plasma cushions in the hole-boring scenario," Plasma Phys. Controlled Fusion **55**, 095016 (2013).

[40]N. V. Elkina, A. M. Fedotov, I. Yu. Kostyukov, M. V. Legkov, N. B. Narozhny, E. N. Nerush, and H. Ruhl, "QED cascades induced by circularly polarized laser fields," Phys. Rev. Spec. Top.–Accel. Beams **14**, 054401 (2011).

[41]L. D. Landau, J. S. Bell, M. J. Kearsley, L. P. Pitaevskii, E. M. Lifshitz, and J. B. Sykes, *Electrodynamics of Continuous Media* (Elsevier, 2013), Vol. 8.

[42]See ipfran.ru/institute/structure/421969/quill-3d-code for QUILL code.

[43]A. Di Piazza, C. Müller, K. Z. Hatsagortsyan, and C. H. Keitel, "Extremely high-intensity laser interactions with fundamental quantum systems," Rev. Mod. Phys. **84**, 1177–1228 (2012).

[44]S. S. Bulanov, C. B. Schroeder, E. Esarey, and W. P. Leemans, "Electromagnetic cascade in high-energy electron, positron, and photon interactions with intense laser pulses," Phys. Rev. A **87**, 062110 (2013).

[45]A. Mironov, A. Fedotov, and N. Narozhny, "Observable features of QED cascades in collisions of GeV electrons with intense laser pulses," J. Phys.: Conf. Ser. **826**, 012029 (2017).

[46]L. D. Landau, *The Classical Theory of Fields* (Elsevier, 2013), Vol. 2.

[47]J. N. Bardsley, B. M. Penetrante, and M. H. Mittleman, "Relativistic dynamics of electrons in intense laser fields," Phys. Rev. A **40**, 3823 (1989).

©Author(s) 2021